From the example in the previous section, enhancing efficiency for convolution in the presence of nonlinear terminations is crucial, since it takes up most of the run time. Although we only confine ourselves to the *S*-parameter application here, other parameters such as the *Z* or *Y* matrix, preferred for RLC circuits, can also be used easily. Moreover, this algorithm can be directly incorporated into multiconductor transmission lines (MTL) terminated with nonlinear loads [1] as well.

REFERENCES

1. A.R. Djordjevic, T.K. Sarkar, and R.F. Harrington, Analysis of lossy transmission lines with arbitrary nonlinear terminal networks, IEEE Trans Microwave Theory Tech MTT-34 (1986), 660–666.
2. J.E. Schutt-Aine and R. Mittra, Scattering parameters transient analysis of transmission lines loaded with nonlinear terminations, IEEE Trans Microwave Theory Tech 36 (1988), 529–536.
3. E. Hairer, C. Lubich, and M. Schlichte, Fast numerical solution of nonlinear Volterra convolution equations, SIAM J Sci Stat Comput 6 (1985), 532–541.
4. E. Hairer, C. Lubich, and M. Schlichte, Fast numerical solution of weakly singular Volterra equations, J Comp Appl Math 23 (1988), 87–98.
5. D.M. Pozar, Microwave engineering, 2nd ed., Wiley, New York, 1998.
6. W.H. Press et al., Numerical recipes in C, 2nd ed., Cambridge Press, Cambridge, UK, 1999.

NEAR-FIELD IMAGING BY NEGATIVE PERMITTIVITY MEDIA

W. T. Lu and S. Sridhar
Department of Physics
Northeastern University
Boston, MA 02115

Received 2 May 2003

ABSTRACT: *The imaging of the near field by a slab of negative permittivity medium is discussed. The performance of this flat lens is limited by the working wavenumber* k_0 *and the slab thickness* d. *For* $k_0 d \ll 0.937$, *the resolution of the flat lens can be smaller than the wavelength and depends logarithmically on* $1/k_0 d$. *The electric field is finite everywhere, but will diverge algebraically as one reduces* $k_0 d \to 0$. © 2003 Wiley Periodicals, Inc. Microwave Opt Technol Lett 39: 282–286, 2003; Published online in Wiley InterScience (www.interscience.wiley.com). DOI 10.1002/mop.11191

Key words: *near-field imaging; evanescent waves; negative permittivity; refraction; transmission*

1. INTRODUCTION

The idea of negative refraction came to life when Veselago [1] pointed out the possible existence of negative-index media (NIM) without violating Maxwell's equations. Based on the idea of negative refraction, Pendry [2] proposed that a flat slab of such a medium can focus an object on the other side of the slab. Not only the far field (which constitutes of propagating plane waves), but also the near field of an object can be focused through such a slab. This enables one to circumvent the diffraction limited resolution and allows for subwavelength imaging. The proposal of this "perfect lens" led to growing interest and also initiated some controversy [3–5]. It is now becoming clear that the idea of a perfect lens is physically sound [6, 7] and also experimentally feasible in systems such as metamaterials [8, 9] and photonic crystals [10].

PACS numbers: 78.20.Ci, 41.20.Jb, 42.25.-p, 42.30.-d.

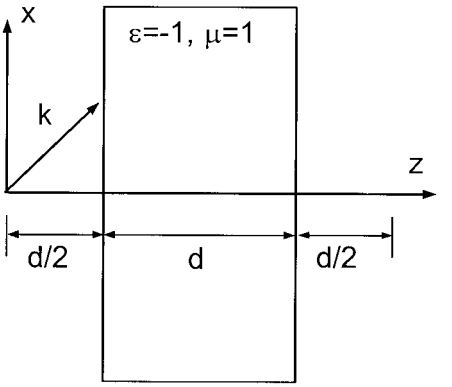

Figure 1 Sketch of a flat lens with $\varepsilon = -1$, $\mu = 1$, and slab thickness d

Pendry also noticed that a flat slab of material which has negative permittivity ($\varepsilon < 0$) can act as a lens to focus the near field. The near-field optical technique has been pushed to have a spatial resolution of about 20 nm [11] at optical frequencies. In this paper, we discuss the near-field imaging of this lens with negative permittivity $\varepsilon < 0$. To have the best focus of the near field, it is desirable for the slab to have permittivity $\varepsilon(\omega) = -1$ at a certain frequency. As required by causality, no material can have static permittivity $\varepsilon(\omega = 0) = -1$. Only at a certain nonzero frequency ω_0 and nonzero wave number $k_0 = \omega_0/c$, $\varepsilon = -1$ can this be realized. This will happen when one crosses a resonant frequency in the case of plasma $\varepsilon(\omega) = 1 - \omega^2/\omega_p^2$, with ω_p the plasma frequency. This flat lens with $\varepsilon = -1$ will amplify the *P*-polarized evanescent waves, thus the diffraction limit of the ordinary lens which only focuses propagating waves, will be broken. In order to focus the *S*-polarized near field, one needs material with negative permeability $\mu(\omega) = -1$. As pointed by Landau [12], at very high frequencies such as at optical frequencies, $\mu \to 1$. So, a flat lens of any medium is not likely to focus the *S*-polarized near field in optical frequencies.

The presence of nonzero k_0 will put strong restrictions on the performance of the lens. As $k_0 \to 0$, the lens will focus more details of the near field. In this paper, we discuss in depth the limitation of the superlens due to finite k_0. Shen and Platzman considered the imaging of a point dipole [13]. Here, we give a detailed discussion through the example of the imaging of two-spike source, which was also discussed by Pendry [2]. The divergence of the field in the limit $k_0 \to 0$ will also be discussed.

2. SLAB REFRACTION OF *P*-POLARIZED PLANE WAVES

To begin with, we consider a plane wave with *P*-polarization. The incident electric field is given by

$$\mathbf{E}_0(k_x) = e^{ik_x x + ik_z z}(k_x \hat{\mathbf{z}} - k_z \hat{\mathbf{x}}). \tag{1}$$

Let the thickness of the slab be d. In our coordinate system, the z axis is along the direction from a vacuum to the slab and the x axis is along the interface, as shown in Figure 1. We place a source at $z = 0$, the first interface of the slab at $z = d/2$, and the second at $z = 3d/2$. At this moment, we treat the slab as ordinary dielectrics. The field configuration of the slab refraction can be obtained using standard methods [14]. The reflected and transmitted electric fields are

$$\mathbf{E}_r(k_x) = R_P e^{ik_x x + ik_z(d-z)}(-k_x\hat{\mathbf{z}} - k_z\hat{\mathbf{x}}), \quad (2)$$

$$\mathbf{E}_t(k_x) = T_P e^{ik_x x + ik_z(z-d)}(k_x\hat{\mathbf{z}} - k_z\hat{\mathbf{x}}), \quad (3)$$

with the reflection and transmission coefficients

$$R_P = \frac{(1-T^2)\Gamma}{1-\Gamma^2T^2},\ T_P = \frac{(1-\Gamma^2)T}{1-\Gamma^2T^2}, \quad (4)$$

and

$$\Gamma = (\varepsilon k_z - k_{rz})/(\varepsilon k_z + k_{rz}),\ T = \exp(ik_{rz}d). \quad (5)$$

Here $k_z = \sqrt{k_0^2 - k_x^2}$ is the z component of the wave vector in vacuum and $k_{rz} = \sqrt{n^2k_0^2 - k_x^2}$ is that inside the slab. The electric field inside the slab is

$$\mathbf{E}_s(k_x) = \frac{e^{ik_x x + ik_z d/2 + ik_{rz}(z-d/2)}}{1-\Gamma^2T^2} \times \left[\frac{1-\Gamma}{\varepsilon}(1+\Gamma T^2 e^{ik_{rz}(d-2z)})\hat{\mathbf{z}} - (1+\Gamma)(1-\Gamma T^2 e^{ik_{rz}(d-2z)})\frac{k_z}{k_x}\hat{\mathbf{x}}\right]. \quad (6)$$

The propagating plane waves will become evanescent when $k_x > k_0$, so that k_z is purely imaginary, that is, $k_z = i\sqrt{k_x^2 - k_0^2}$. These near-field waves cannot propagate and will decay exponentially around the object in the vacuum along the z axis. For those evanescent waves, the magnetic field is exponentially small, compared with the electric field. Thus, practically, there is only electric field, as in the electrostatic case. The energy density of the incident evanescent plane wave around the source in the vacuum is $u = e^{2ik_z z}/4\pi$.

The above expressions of the slab refraction is valid for arbitrary ε and μ. For NIM with $\varepsilon = -1$ and $\mu = -1$, since $k_{rz} = k_z$, the denominator of Γ in Eq. (5) is zero; thus, $\Gamma \to \infty$. The evanescent wave will be amplified since the transmission coefficient $T_P = \exp(\sqrt{k_x^2 - k_0^2}d)$ will grow exponentially with the slab thickness and increasing k_x. This amplifying factor will compensate the decay in the vacuum such that at a distance $d/2$ away from the second surface of the slab, $T_p\exp(ik_z d) = 1$. Hence all the evanescent waves will be amplified through the slab and a perfect image of the object at $z = 0$ is obtained at $z = 2d$.

3. PROPERTIES OF TRANSMISSION AND REFLECTION COEFFICIENTS FOR EVANESCENT WAVES

Here we consider a slab with $\varepsilon = -1$ and $\mu = 1$. A slab of metal at certain frequencies will have this property. Although this lens will not perfectly focus all the evanescent waves, it can recover part of the evanescent waves under certain conditions. The slab will still be able to achieve subwavelength imaging. Since in this case the index of refraction is purely imaginary with $n = i$, the z component of the wave vector for the evanescent wave is $k_{rz} = i\sqrt{k_x^2 + k_0^2}$. To proceed, we define $\delta = k_x/k_0$, which is greater than unity for evanescent waves. From the expression of Γ in Eq. (5), one obtains $\Gamma = -(\delta^2 + \sqrt{\delta^4 - 1}) < -1$. Unlike in the case for NIM with $\varepsilon = -1$ and $\mu = -1$, here Γ is finite.

We first look at the property of T_P. From the expression in Eq. (3) of $\mathbf{E}_t(k_x)$, one can see that if $T_p\exp(ik_z d) = 1$, then $\mathbf{E}_t(k_x)$ with $z \geq 2d$ will be exactly the same as $\mathbf{E}_0(k_x)$ with $z \geq 0$. Here the factor $\exp(ik_z d)$ is the damping factor, due to the propagation of the evanescent waves in the vacuum. Since $\Gamma < 0$, T_P will diverge at $\Gamma T = -1$. This condition can be re-expressed in terms of δ in the following equation:

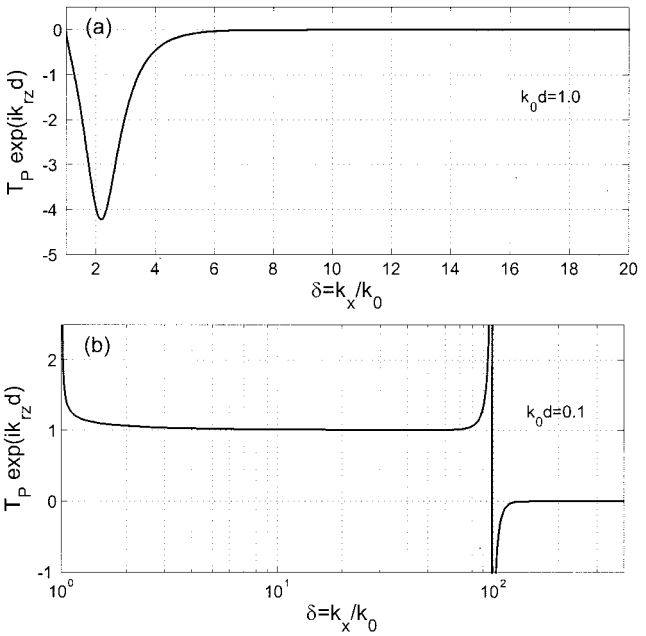

Figure 2 Plot of $T_p\exp(ik_z d)$ for (a) $k_0 d = 1.0$, (b) $k_0 d = 0.1$

$$k_0 d = [\ln(\delta^2 + \sqrt{\delta^4 - 1})]/\sqrt{\delta^2 + 1}. \quad (7)$$

The maximum of the function on the right side of above equation is about 0.937 261 at $\delta \simeq 2.356\,574$. So if $k_0 d > 0.937$, $-1 < \Gamma\exp(ik_{rz}d) < 0$, there is no singularity in T_p with $T_p\exp(ik_z d)$ being negative, as can be seen in Figure 2(a) with $k_0 d = 1.0$. Even though the maximum of $|T_p\exp(ik_z d)|$ can be much larger than 1, $|T_p\exp(ik_z d)|$ is not very flat. Evanescent waves with different k_x will have different amplifying factors. For a source with many component of k_x, the transmitted evanescent waves will be severely distorted. So there is no subwavelength imaging for $k_0 d > 0.937$. On the other hand, if $k_0 d < 0.937$, Eq. (7) will give two solutions, δ_1 and δ_2, for δ with $\delta_1 < \delta_2$. If $k_0 d \ll 0.937$, one has $\delta_1 \to 1$ and $\delta_2 \simeq -2\ln(k_0 d)/k_0 d$. If $k_x > k_x^{\max} \equiv \delta_2 k_0 \simeq -2\ln(k_0 d)/d$, except in the vicinity of $k_x^{\max}$, $T_p\exp(ik_z d)$ decays exponentially to zero with increasing k_x. More specifically, for $k_x \gg k_x^{\max}$, one has $\Gamma T \to 0$, so that $T_p \sim 4\delta^4 e^{-k_x d}$. Details of the object with high Fourier components $k_x > k_x^{\max}$ will be lost in the imaging process. What is amplified through the slab is a finite range of Fourier components, $k_x \in (k_x^{\min}, k_x^{\max})$ with $k_x^{\min} \equiv \delta_1 k_0$. Within this range, except in the vicinity of $k_x^{\min}$ and $k_x^{\max}$, $T_p\exp(ik_z d)$ is very flat and $T_p\exp(ik_z d) \simeq 1$. This can be seen in Figure 2(b) with $k_0 d = 0.1$. In the neighborhood of $k_0 d \sim 0.937$, the lens cannot focus, even though some components of the evanescent waves do become amplified through the slab.

The reflection coefficient R_P has similar behavior as T_P. From the expression of T_P and R_P, the difference between them is $T_P - R_P = (T - \Gamma)/(1 - \Gamma T)$. Since $\Gamma T < 0$, there is no singularity in $T_P - R_P$. The difference will diverge exponentially for evanescent waves with $k_x \to \infty$. The behavior of $R_P\exp(ik_z d)$ for different values of $k_0 d$ is shown in Figure 3. For finite $k_0 d \ll 0.937$, $R_P\exp(ik_z d)$ is flat with nonzero values for $k_x^{\min} \ll k_x \ll k_x^{\max}$. This is due to the mismatch of the surface impedance between the vacuum ($\sqrt{\varepsilon/\mu} = 1$) and the slab ($\sqrt{\varepsilon/\mu} = i$). Unlike the behavior of T_P, which decays exponentially for large k_x, the amplitude of R_P increases as $|R_P| \sim 2\delta^2$ for $k_x \gg k_x^{\max}$ with $k_0 d \ll 0.937$.

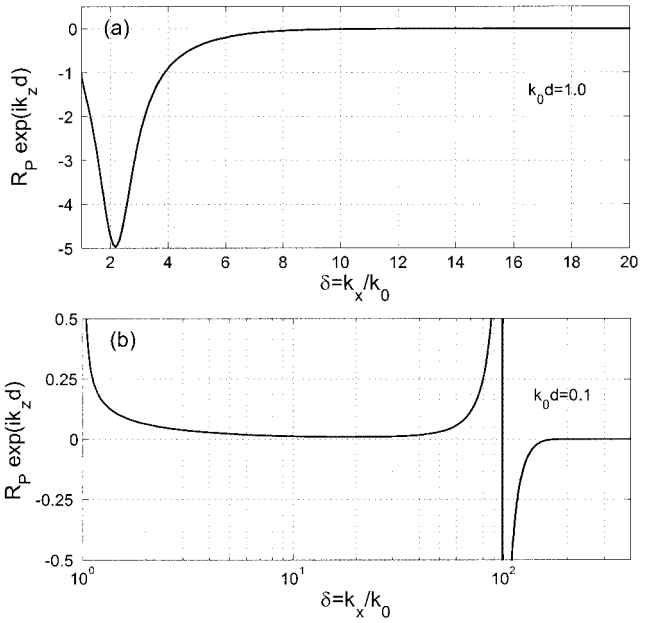

Figure 3 Plot of $R_p\exp(ik_zd)$ for (a) $k_0d = 1.0$, (b) $k_0d = 0.1$

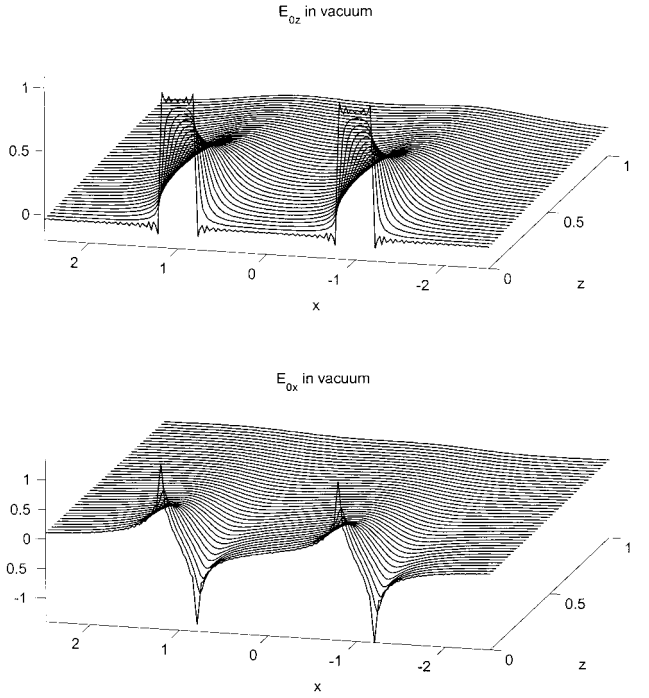

Figure 4 The near field of the two-spike object, E_{0z} (top) and E_{0x} (bottom) with $a = 0.2$, $b = 1$, $d = 1$, and $k_0d = 0.1$

4. NEAR FIELD IMAGING OF A TWO-SPIKE OBJECT

To illustrate the performance of the above lens, we take as an example the two-spike object [2]. The electric field is

$$\mathbf{E}_0 = \int_0^\infty dk_x v_{k_x} e^{ik_z z}\left(\hat{\mathbf{z}}\cos k_x x - i\hat{\mathbf{x}}\frac{k_z}{k_x}\sin k_x x\right), \tag{8}$$

with the coefficient v_{k_x} given by

$$v_{k_x} = (4/\pi k_x)\sin k_x a \cos k_x b. \tag{9}$$

Here, $2b$ is the distance between the two spikes and $2a$ is the individual spike width. The waves will propagate freely in the vacuum for $k_x < k_0$. Since k_z is purely imaginary for evanescent waves with $k_x > k_0$, the near field part of $\mathbf{E}_0$ of the two-spike object is real as expected, which is illustrated in Figure 4.

The transmitted near field can be obtained by the integration of Eq. (3) with v_{k_x}/k_x over k_x. For the source shown in Figure 4, the transmitted near field is shown in Figure 5 with $k_0d = 0.1$. The reflected field and the field inside the slab can also be obtained similarly. The near field distribution in the vicinity of the slab with $k_0d = 0.1$ is shown in Figure 6. One notices that there is quite a lot of field accumulated around the two surfaces. The amplitude of the field around the two surfaces reaches about 40, as compared with that of the source, which reaches 1 (this will be explained subsequently).

The imaging performance for slabs with different values of k_0d is shown in Figure 7. One can see that, as the value of k_0d is increased, the two spikes at the imaging plane $z = 2d$ will be less distinguishable. When the value of k_0d is close to and beyond 0.937, the slab lens loses the power to amplify evanescent waves and the two spikes disappear.

In order to address the issue of singularity of the near-field imaging, we consider the electrostatic limit $k_0 \to 0$. In this limit, we assume that $\varepsilon = -1$ still holds, even though the law of causality will be violated. Subsequently, one has $k_z = k_{rz} = ik_x$. As a result, $\Gamma \to \infty$, and we obtain

$$\mathbf{E}_0 = \frac{2}{\pi}\Re\sum_{\pm}(\hat{\mathbf{z}} - i\hat{\mathbf{x}})\arctan\frac{a}{z - i(x \pm b)},$$

$$\mathbf{E}_t = \frac{2}{\pi}\Re\sum_{\pm}(\hat{\mathbf{z}} - i\hat{\mathbf{x}})\arctan\frac{a}{z - 2d - i(x \pm b)}. \tag{10}$$

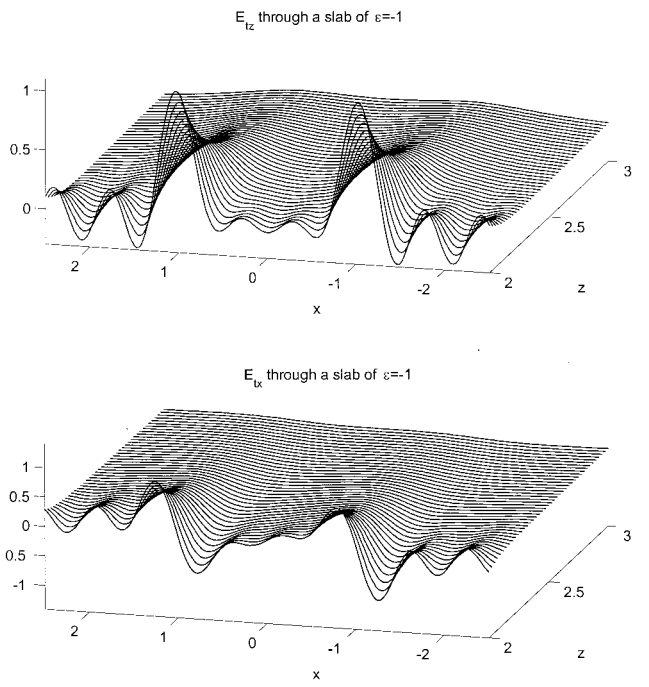

Figure 5 Transmitted near field of the two-spike source (Fig. 4), E_{tz} (top) and E_{tx} (bottom), for $z \geq 2d$

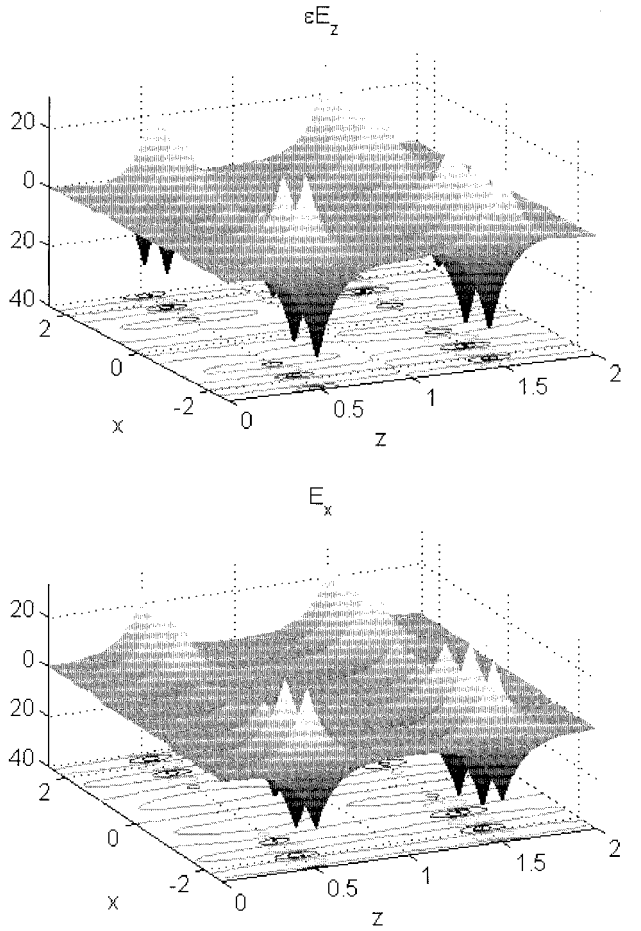

Figure 6 Near-field εE_z (top) and E_x (bottom) in the vicinity of the slab for the two-spike object with $a = 0.2$, $b = 1$, $d = 1$, and $k_0 d = 0.1$

Here, we use the following integral:

$$\int_0^\infty dk\, \frac{\sin ka}{k}\, e^{-k\xi} = \arctan \frac{a}{\xi}, \tag{11}$$

for any complex ξ with $\Re\xi > 0$.

The above expression for $\mathbf{E}_t$ is only valid for $z \geq 2d$. The transmitted electric field $\mathbf{E}_t$ diverges in the region with $z \in (3d/2, 2d)$. The reflected field $\mathbf{E}_r$ diverges for $z \in (0, d/2)$. The field $\mathbf{E}_s$ inside the slab diverges everywhere except on the line $z = d$. The field $\mathbf{E}_s$ on this line is

$$\mathbf{E}_s = \frac{2}{\pi}\Re \sum_{\pm} (\hat{\mathbf{z}} - i\hat{\mathbf{x}}) \arctan \frac{a}{0^+ - i(x \pm b)}.$$

This means that one has a perfect image of the source in the middle of the slab besides another one outside the slab. This scenario is similar to the case of far-field imaging, except that here one has subwavelength imaging.

For any physical material, the dielectric constant should always be positive as one approaches the electrostatic limit. The presence of nonzero k_0 for $\varepsilon = -1$ will remove the divergence which is due to an accumulation of field along the two surfaces of the slab. For small but finite $k_0 d$, the field is bounded and finite everywhere. As one decreases $k_0 d \to 0$, the electric field will diverge. To check the divergence, we consider for example the transmitted field $\mathbf{E}_r$ at $z = d/2$, where the field is more likely to diverge. Since

$$|\mathbf{E}_r| \sim \int_1^{-2\ln k_0 d} d\xi \frac{e^{3\xi/2}}{\xi^3} + \int_{-2\ln k_0 d}^{\infty} d\xi \xi e^{-\xi/2} \sim (k_0 d)^{-3},$$

the electric field around the first surface of the slab will diverge as $E \sim (k_0 d)^{-3}$. For the field around the second surface, we consider $\mathbf{E}_t$ at $z = 3d/2$. One has

$$|\mathbf{E}_t| \sim \int_1^{-2\ln k_0 d} d\xi \frac{e^{\xi/2}}{\xi} \sim (k_0 d)^{-1}.$$

The electric field around the second surface of the slab will diverge as $E \sim (k_0 d)^{-1}$.

5. CONCLUSION AND DISCUSSION

In summary, we discussed the limitation of the lens made of a slab with negative permittivity. For small $k_0 d$, the lens can focus partially subwavelength details of the P-polarized near field of an object. The resolution of the slab lens depends logarithmically on $(k_0 d)^{-1}$, since $k_x^{\max} \simeq -2\ln(k_0 d)/d$. For fixed k_0, in order for the lens to pick up the high Fourier component of the evanescent waves, one may reduce the slab thickness d such that $k_0 d \ll 0.937$. Given the fact that the minimum thickness of a material under normal condition is about $d \sim 10^{-8}$ cm, the working frequency of the slab lens will be $\omega/2\pi < 5 \times 10^{17}$ Hz, which includes the optical frequency range. At $\omega/2\pi = 3 \times 10^{14}$ Hz with slab thickness $d = 100$ nm, one has $k_0 d = 0.1$ and $k_x^{\max} \simeq 10^8$ m^{-1}, and a spatial resolution of about 60 nm can be obtained. In the limit $k_0 d \to 0$, all the evanescent waves will be amplified; thus, the slab lens will become perfect for near-field imaging. The electromagnetic field is finite everywhere but will diverge algebraically in the limit $k_0 d \to 0$ on the surfaces of the slab lens.

ACKNOWLEDGMENTS

This work was supported by the National Science Foundation NSF-PHY-0098801 and the Air Force Research Laboratories.

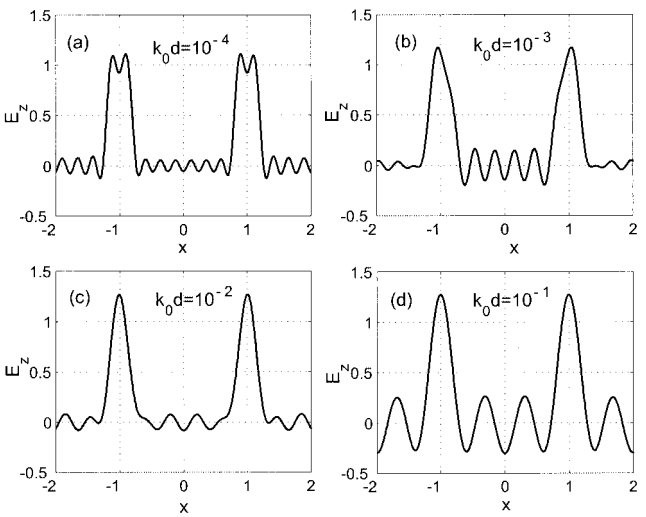

Figure 7 Images of evanescent waves in the plane at $z = 2d$ with $a = 0.2$, $b = 1$, and $d = 1$ for different values of $k_0 d = 10^{-4}$, 10^{-3}, 10^{-2}, and 10^{-1}

REFERENCES

1. V.G. Veselago, The electrodynamics of substances with simultaneously negative values of ε and μ, Soviet Physics USPEKI 10 (1968), 509–514.
2. J.B. Pendry, Negative refraction makes a perfect lens, Phys Rev Lett 85 (2000), 3966–3969.
3. G.W. Hooft, Comment on "Negative refraction makes a perfect lens," Phys Rev Lett 87 (2001), 249701; J.M. Williams, Some problems with negative refraction, Phys Rev Lett 87 (2001), 249703.
4. P.M. Valanju, R.M. Walser, and A.P. Valanju, Wave refraction in negative-index media: Always positive and very inhomogeneous, Phys Rev Lett 88 (2002), 187401.
5. N. Garcia and M. Nieto-Vesperinas, Left-handed materials do not make a perfect lens, Phys Rev Lett 88 (2002), 207403.
6. F.D.M. Haldane, Electromagnetic surface modes at interfaces with negative refractive index make a "not-quite-perfect" lens, arXiv: cond-mat/0206420, 2002.
7. G. Gómez-Santos, Universal features of the time evolution of evanescent modes in a left-handed perfect lens, Phys Rev Lett 90 (2003), 077401.
8. D.R. Smith et al., Composite medium with simultaneously negative permeability and permittivity, Phys Rev Lett 84 (2000), 4184–4187.
9. R.A. Shelby, D.R. Smith, and S. Schultz, Experimental verification of a negative index of refraction, Science 292 (2001), 77–79.
10. C. Luo et al., All-angle negative refraction without negative effective index, Phys Rev B 65 (2002), R201104(4); C. Luo et al., All-angle negative refraction in a three-dimensionally periodic photonic crystal, Appl Phys Lett 81 (2002), 2352–2354.
11. E.J. Sánchez, L. Novotny, and X.S. Xie, Near-field fluorescence microscopy based on two-photon excitation with metal Ti, Phys Rev Lett 82 (1999), 4014–4017; A. Hartschuh et al., High-resolution near-field Raman microscopy of single-walled carbon nanotubes, Phys Rev Lett 90 (2003), 095503(4).
12. L.D. Landau and E.M. Lifshitz, Electrodynamics of continuous media, 2nd ed.
13. J.T. Shen and P.M. Platzman, Near-field imaging with negative dielectric constant lenses, Appl Phys Lett 80 (2002), 3286–3288.
14. J.D. Jackson, Classical electrodynamics, 2nd ed., Wiley, New York, 1975.

HIGH-POWER DUAL-WAVELENGTH LOOP-MIRROR CAVITY FIBER LASER

F. Abdullah, M. A. Mahdi, B. Bouzid, and M. K. Abdullah
Photonics and Fiber Optics System Laboratory
Department of Computer and Communication Systems Engineering
Universiti Putra Malaysia
43400 Serdang, Selangor, Malaysia

Received 6 May 2003

ABSTRACT: *A high-power dual-wavelength laser is constructed in two fiber-loop mirror cavities by utilizing a common-gain medium. The output power and side-mode suppression ratio (SMSR) of the lasers were investigated for a bidirectionally pumped system. The outcome of the experiment shows that two lasing signals can be obtained at the wavelengths of 1546.04 and 1550.64 nm at a less than 1-dB peak power difference, at peak powers of 7.30 and 6.57 dBm, respectively. This result was obtained without any intracavity attenuators. The side-mode suppression ratio of both signals is around 46 dB.* © 2003 Wiley Periodicals, Inc. Microwave Opt Technol Lett 39: 286–287, 2003; Published online in Wiley InterScience (www.interscience.wiley.com). DOI 10.1002/mop.11192

Key words: *dual wavelength; fiber laser; high power; loop mirror; power difference*

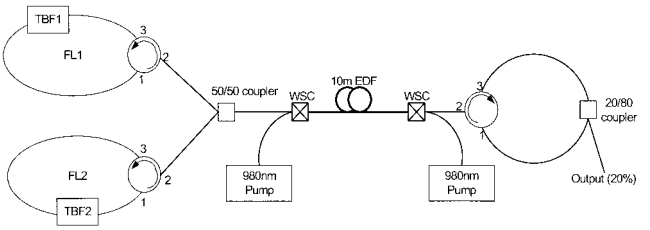

Figure 1 Configuration of the dual wavelength bidirectional pumped dumbbell EDFL

INTRODUCTION

Multiple-wavelength optical sources have been investigated as one of the promising technologies for applications in wavelength division multiplexed (WDM) systems. Many techniques have been employed in designing a laser system emitting multiple wavelengths using erbium-doped fiber laser (EDFL). Park et al. [1] used eight fiber-loop mirrors (FLMs) to produce eight wavelengths. However, the output power of all the channels is not equal and is relatively low. Another technique to produce multiple wavelengths involves the use of a twin core erbium-doped fiber (EDF) [2]. The output wavelengths are selected by using fiber Bragg gratings (FBGs). However, the EDF used is a highly specialized fiber that is costly, and the output power reported with this technique is relatively low. Another approach is to use a periodic filter to produce multiple wavelengths [3]. To prevent single-frequency lasing, a frequency shifter is introduced in the ring cavity. It requires two gain media to compensate the loss introduced by the frequency shifter. This approach is rather complicated. A high-power output dual-wavelength laser is also reported in [4]. However, the output is taken from two fibers, instead of one. Recently, a linear cavity configuration using cascaded FBG and EDF has been reported [5]. The output power of the multiple lasers is considerably high; however, this technique does not deploy a single EDF coil. Furthermore, the reflectivity of the FBGs are used to create an equal net gain of the laser system at multiple wavelengths.

In this paper, a new and simple configuration utilizing FLMs with an intraloop tunable bandpass filter (TBF) is proposed. The signals share most of the cavities, thus reducing the cavity discrepancy. This includes a common section of EDF to provide amplification for both lasing wavelengths. In this configuration, the two signals have almost equivalent characteristics in terms of power and side mode suppression ratio (SMSR) at certain wavelengths. The 1-dB difference peak power produced by this system is higher than previously reported results for a system employing relatively low pump power, and short EDF with low-ion concentration.

EXPERIMENTAL CONFIGURATION

The setup for this experiment follows a dumbbell-shaped configuration, as shown in Figure 1. The left side of the dumbbell has been modified, such that it consists of two FLMs. The amplified spontaneous emission (ASE) signal will only pass through it in one direction via a three-port circulator. The directivity loss for port 3–1 is around 65 dB, which is enough to prevent the signal from taking the shortcut through it. Two other ports have 1-dB insertion loss each. Therefore, the ASE signal enters the loop from port 2–3 and propagates through the TBF and out of the loop via port 1–2. A fused fiber coupler is used to obtain the laser output at the 20% port. The EDF used is 10-m long with a core diameter of 2 μm and erbium concentration of 440 ppm. Both of the TBFs have a 3-dB passband of 1 nm and tunable from 1525 nm to 1565 nm.

On first pass, the ASE is equally split into the two loops. In each loop, most of the ASE signal will be filtered out, and only the